Editors' Suggestion

Subkilohertz optical homogeneous linewidth and dephasing mechanisms in Er^{3+}:Y_2O_3 ceramics

Rikuto Fukumori,[1] Yizhong Huang,[1] Jun Yang,[2] Haitao Zhang,[2] and Tian Zhong[1,*]
[1]*Pritzker School of Molecular Engineering, University of Chicago, Chicago, Illinois, 60637, USA*
[2]*Corning Research & Development Corporation, Sullivan Park, Painted Post, New York 14870, USA*

(Received 12 November 2019; accepted 18 May 2020; published 8 June 2020)

We report an optical homogeneous linewidth of 580 ± 20 Hz of Er^{3+}:Y_2O_3 ceramics at millikelvin temperatures, narrowest so far in rare-earth doped ceramics, as well as a slow spectral diffusion of ∼2 kHz over a millisecond time scale. Detailed investigations of temperature and field dependence of optical coherence and spectral diffusions reveal the remaining weak dephasing mechanisms as coupling to elastic two-level systems and superhyperfine interactions of Er^{3+} with nuclear spins. The measured transient coherence properties can be understood in part from frozen Er^{3+} spins at dilution temperatures. In addition to informing possible refinement in material synthesis to further suppress dephasings, these spectroscopic results put Er^{3+}:Y_2O_3 ceramics as a promising candidate for quantum systems.

DOI: 10.1103/PhysRevB.101.214202

I. INTRODUCTION

Solids doped with trivalent rare-earth ions are increasingly important quantum materials as the dopants exhibit optical transitions with narrow homogeneous linewidths and spins with long coherence times at cryogenic temperatures [1–5]. These spectroscopic properties make rare-earth-ion doped materials appealing for applications such as optical quantum memories [6] for long-distance quantum networks [7], optical-microwave quantum transductions [8], and potentially nanoscopic quantum sensing [9].

While bulk single crystals are the most common hosts for rare-earth dopants [4,10], other platforms including nanocrystals and ceramics have been attracting significant interests as these materials are relatively easy to synthesize, and they exhibit coherence properties approaching or on par with bulk crystal counterparts. In particular, Y_2O_3 is a host matrix with low nuclear magnetic moments. Its simpler chemical composition and lattice structure allows synthesis of micro/nanostructured Y_2O_3 in different topologies using bottom-up approaches [11], including thin films [12], nanoparticles [13,14], and ceramics [15], with increasingly good control of the material volume, particle sizes, and doping concentrations. Rare-earth doped Y_2O_3 has already shown excellent coherence characteristics. Near radiatively limited optical homogeneous linewidth of $\Gamma_h = 760$ Hz was reported in single crystal Eu^{3+}:Y_2O_3 [16]. $\Gamma_h = 85.6$ kHz was reported for Eu^{3+}:Y_2O_3 nanoparticles [17] and $\Gamma_h = 4$ kHz for transparent ceramics [18]. Additionally, $\Gamma_h = 108$ kHz and spin $T_2 = 880$ μs was reported in Pr^{3+}:Y_2O_3 nanoparticles [14]. Recently, a narrow inhomogeneous linewidth of 430 MHz and $\Gamma_h = 11.2$ kHz in the telecom band was demonstrated in Er^{3+}:Y_2O_3 [15]. Since optical homogeneous linewidths are correlated with spin coherences, measurements of Γ_h offer a wealth of information on the spin coherence and dynamics. The narrower the linewidth, the better resolution to reveal weak dephasing interactions of dopant spins with the host environment. This understanding of dephasing mechanisms provides insights for control of dopant spins and optimization of the material synthesis to realize desired quantum characteristics.

To this end, we measure optical coherence properties of the ${}^4I_{13/2}(Y_1) \rightarrow {}^4I_{15/2}(Z_1)$ transition in transparent Er^{3+}:Y_2O_3 ceramics. Er^{3+} is a paramagnetic ion with a half-integer spin (Kramers ion) with an optical transition in the low-loss telecommunication *C* band. An exceptionally narrow optical homogeneous linewidth (Γ_h) of 73 Hz [4] and a long hyperfine spin coherence time of 1.3 s [5] have been measured in Er^{3+}:Y_2SiO_5 and $^{167}Er^{3+}$:Y_2SiO_5 bulk crystals, respectively. Meanwhile, Er^{3+} has a large gyromagnetic ratio, up to $g = 15$ in Er^{3+}:Y_2SiO_5 [19] and $g = 12$ in Er^{3+}:Y_2O_3 [20], which allows strong coupling to magnetic fields that is potentially advantageous for microwave-optical transduction or sensing applications. On the other hand, the strong magnetism of Er^{3+} imposes challenges to attain long coherence lifetimes due to undesired interactions with other Er^{3+} ions, phonons, and impurities in the host. Consequently, previous results of long coherence lifetimes were obtained by applying a very large field of a few teslas to strongly suppress these interactions [4,5], or by freezing Er^{3+} electronic spins at dilution temperatures. This latter technique has been applied to Er^{3+}:$LiYF_4$ [21] and Er^{3+}:Y_2SiO_5 single crystals [22].

Here we report the narrowest optical homogeneous linewidth measured so far in rare-earth doped ceramics of 580 Hz at an applied magnetic field of 0.7 T in the < 100 mK temperature regime. The measured optical transition shows a slow spectral diffusion of ∼2 kHz over 1 ms. We then systematically investigate field, temperature dependence of Γ_h and spectral diffusions to determine the dephasing mechanisms, and quantify the remaining broadening due to coupling to elastic two-level systems (TLS) and nuclear spins. Our results of a subkilohertz optical linewidth with a slow spectral diffusion of Er^{3+}:Y_2O_3 demonstrates a significant potential of

*Corresponding author: tzh@uchicago.edu

this material for quantum technologies. The evidence of TLS coupling indicates the prospect of further suppressing dephasing with larger grain sizes in the ceramics, and a potential to realize hybrid quantum systems based on rare-earth spins and long-lived TLS.

II. EXPERIMENTAL METHODS

The material under study is transparent 20 parts per million (ppm) doped Er^{3+}:Y_2O_3 ceramics, with dimensions of $9.5 \times 3 \times 1.7$ mm^3. This material is made by sintering Er^{3+} doped Y_2O_3 nanoparticles (40 nm) in the following way. The nanoparticles are pressed into a pellet in a steel die at approximately 8 klbs force. This pellet is isostatically pressed at 25 kpsi in a latex isopressing sheath at room temperature, followed by sintering at 1500 °C in air for 2 h. The pellet is then hot isostatically pressed (HIP) at 1490 °C for 16 h at 29 kpsi under an argon atmosphere in a graphite furnace. The pellet is buried inside Y_2O_3 powder during HIP to reduce carbon contamination which comes from the graphite furnace. The surface of the sample is polished with a roughness of about 5 nm. This resulted in polycrystals with an average cross-sectional grain size of 0.3 μm^2. Further details of the sample and manufacturing process are outlined in [15].

A fiber-coupled telecom diode laser (Toptica CTL 1500) was used for optical measurements. Two cascaded fiber-based acousto-optic modulators (AOM) were used to modulate the frequency and intensity of the laser, giving a 100 dB extinction ratio. The light is sent through a fiber-based circulator, which separated the input and output light from the sample.

The sample was mounted on the mixing chamber stage (MXC) of a dilution refrigerator, and a three-axis nanopositioner was used for sample optical alignment. Two copper clips were used to secure the sample on a copper stage for increased thermal conductivity. The light exiting the fiber was focused onto the sample with an aspheric doublet, down to a spot size of 12 μm, and reflected off the gold-coated sample stage and back into the fiber. This created a double pass configuration through the sample. The percentage of the light exiting the fiber to the light collected back by the fiber was about 30%. A superconducting 6-1-1 T vector magnet was mounted around the sample. Because the sample is ceramic and has no preferred crystallographic directions, the magnet was operated only along one (6 T) axis.

For lifetime measurements, photoluminescence excitation (PLE) was measured by sending a 1.5 μs excitation pulse, gated by two AOMs, and the reflection detected by a superconducting nanowire single photon detector (SNSPD). The dark count rate of the SNSPD was measured to 50 ± 10 Hz, and the detector efficiency was about 80%. For absorption spectroscopy, the light was sent to the sample without AOMs, and the reflection was measured with a photodiode.

For optical coherence spectroscopy, two pulse and three pulse photon echoes with heterodyne detection was used. The light before the AOM was split with a fiber-based 50:50 beamsplitter, and one path was sent through an AOM and to the sample, while the other path was used as the local oscillator (LO). The reflection from the sample and the LO was recombined with another 50:50 fiber-based beamsplitter, and the beating at 200 MHz was observed with a photodiode. A variable attenuator and polarization controller was used in the LO path to optimize the echo intensity.

III. RESULTS

A. Optical absorption spectroscopy

Figure 1(a) shows the energy diagram for the ${}^4I_{13/2}(Y_1) \rightarrow {}^4I_{15/2}(Z_1)$ optical transition in the C_2 crystal symmetry site. Application of a magnetic field splits each of these crystal field levels into two Zeeman levels. The g tensor for Er^{3+}:Y_2O_3 crystals was measured in [20]. For polycrystalline ceramics, the Er^{3+} ions are randomly oriented, and thus experience different g factors. We see this in the broadening of the inhomogeneous linewidth with applied magnetic field, as shown in Fig. 1(b). Groups of ions with different g factors spread out in the frequency domain, due to a distribution of $|g_g - g_e|$ values. We measure the optical coherence properties at frequencies corresponding to maximum optical absorption, as indicated by the black line in Fig. 1(b).

The zero-field absorption spectrum for the Y_1-Z_1 transition is shown in Fig. 1(c). This yielded a center frequency of 195 227.0 GHz (1535.61 nm) and a peak absorption coefficient of 3.4 cm^{-1}. The zero field optical inhomogeneous linewidth was 400 MHz full-width-at-half-maximum, which is an order of magnitude narrower than those reported in similar europium doped ceramics [23], and still narrower than previously reported Er^{3+}:Y_2O_3 single crystals [1]. This indicates the low disorder and high purity of the ceramics.

The oscillator strength f is given by [24,25]

$$f = 4\pi\epsilon_0 \frac{9m_e cn}{\pi e^2 N(n+2)^2} \int \alpha(\nu) d\nu, \tag{1}$$

where ϵ_0 is the vacuum permittivity, e is the electron charge, m_e is the electron mass, c is the speed of light, n is the index of refraction, N is the number density of the dopant, and $\alpha(\nu)$ is the absorption coefficient at a certain frequency. Given $\alpha(\nu)$ measured in Fig. 1(c) and the index for Y_2O_3 at 1535 nm $n = 1.9$, we calculate $f = (2.9 \pm 0.3) \times 10^{-7}$, where the uncertainty comes from a 10% uncertainty in the doping level N, and 3% uncertainty from the fit in Fig. 1(c). From this we calculate the spontaneous emission time T_{spon} for the Y_1-Z_1 transition using [26]

$$T_{\text{spon}} = \frac{m_e \epsilon_0 c^3}{2\pi n^2 e^2 \nu^2 f}, \tag{2}$$

which gives $T_{\text{spon}} = 34 \pm 4$ ms.

Figure 1(d) shows a PLE decay integrated over 10 s. The plot is fitted to a single exponential, yielding an excited state lifetime (T_1) of 7.3 ms. We confirmed that reabsorption of emitted photons due to large optical depths was not causing lengthening of the lifetime, by measuring the lifetimes at detuned frequencies where the optical depth was lower. From the measured optical lifetime, we obtain a branching ratio for the Y_1-Z_1 transition as $T_1/T_{\text{spon}} = 0.22 \pm 0.03$.

B. Optical decoherence

We measure the optical coherence using two-pulse photon echoes width heterodyne detection. The π pulse was 500 ns long, and the Rabi frequency was about 1 MHz. The inset of

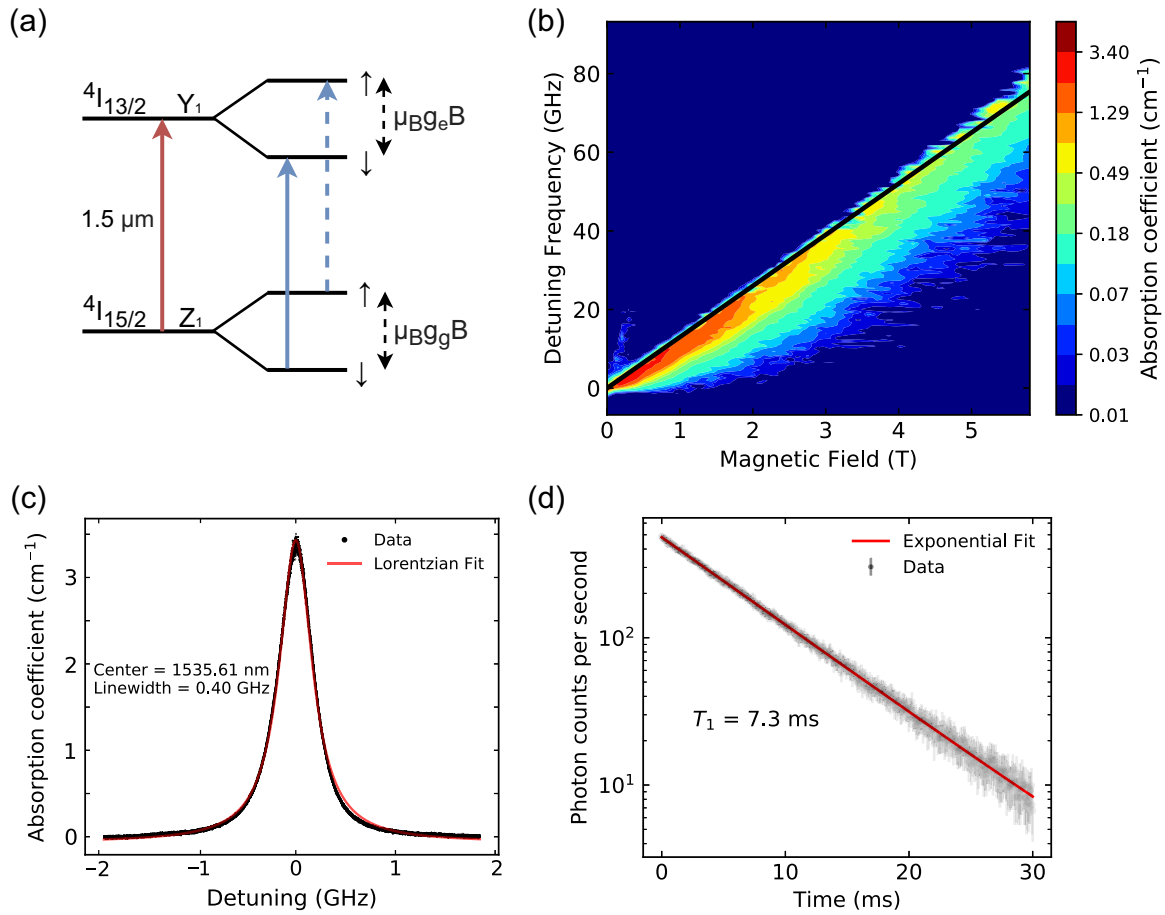

FIG. 1. (a) Energy level diagram for the crystal field $^4I_{13/2}(Y_1) \rightarrow {}^4I_{15/2}(Z_1)$ transition (red arrow) for Er^{3+}. An external magnetic field splits both levels into Zeeman doublets. At low temperatures, most ions occupy the lower spin levels, thus the dominant transition is indicated by the solid blue arrow. (b) Photoluminescence excitation (PLE) spectra as a function of magnetic field and frequency. The line shape gradually broadens with increasing field. With the external field along the crystal z axis, the slope of a contour is proportional to $(g_g - g_e)_z$ and the solid black line indicates the line of maximum absorption, with $(g_g - g_e)_z = 1.84$. (c) Zero-field inhomogeneous linewidth measured by absorption spectroscopy. The data are fitted by a Lorenztian, with a full-width-at-half-maximum of 0.40 GHz. (d) Optical lifetime, measured with PLE detected by a SNSPD, integrated over 10 s. The curve is fitted to a single exponential decay, giving a $T_1 = 7.3$ ms.

Fig. 2 shows typical photon echo decays at various applied fields, along the black line in Fig. 1(b). At all fields, we observed nonexponential decays, which we fit with the Mims decay [27]

$$E(\tau) = E_0 e^{-(2\tau/T_M)^x}, \tag{3}$$

where τ is the delay between the two pulses, x is the parameter describing spectral diffusion, and T_M is the phase memory time. From the fit we extract the effective homogeneous linewidth as $\Gamma_{h,\mathrm{eff}} = 1/(\pi T_M)$. The narrowest linewidth of 580 Hz was observed at 0.7 T.

To determine the dephasing mechanisms, we break down the contributing factors to Γ_h as

$$\Gamma_h = \Gamma_{\mathrm{pop}} + \Gamma_{\text{ion-ion}} + \Gamma_{\text{ion-spin}} + \Gamma_{\mathrm{TLS}} + \Gamma_{\mathrm{phonon}}. \tag{4}$$

Γ_{pop} is the contribution from the excited state radiative lifetime. This gives $\Gamma_{\mathrm{pop}} = 1/2\pi T_1 = 21.8$ Hz, a small contribution to the overall linewidth. $\Gamma_{\text{ion-ion}}$ includes contributions from two factors. One is instantaneous spectral diffusion (ISD) due to strong optical excitations that can abruptly change the local environment [28]. This would cause dephasing with increasing power of the second pulse π. However, we saw no power dependence of the linewidth, suggesting that ISD does not contribute. Furthermore, previous work on a similar sample has shown no change in the linewidth between 2.0 and 11.5 ppm doped samples, further indicating that ISD does not contribute [15]. The second contribution to $\Gamma_{\text{ion-ion}}$ is the resonant Er^{3+}-Er^{3+} flip-flops [29]. From Fig. 1(b) we saw minimal population in the upper Zeeman state at $B >$ 0.1 T. Due to thermal depopulation of the upper Zeeman state, we expect the dephasing from Er^{3+}-Er^{3+} flip-flops to be small.

$\Gamma_{\text{ion-spin}}$ includes dephasing due to the superhyperfine interaction of Er^{3+} with Y^{3+} nuclear spins, and is often the limiting dephasing mechanism, known as the superhyperfine limit [21]. This contribution is usually small, owing to the low nuclear magnetic moment of Y^{3+}, and the large magnetic moment of Er^{3+} creating a frozen core of yttrium whose flipping rates are significantly slowed [21]. Since the magnetic noise of Y^{3+} is independent of field, the characteristic of the superhyperfine limit is a saturation of the homogeneous linewidth above a certain applied magnetic field. $\Gamma_{\text{ion-spin}}$ also

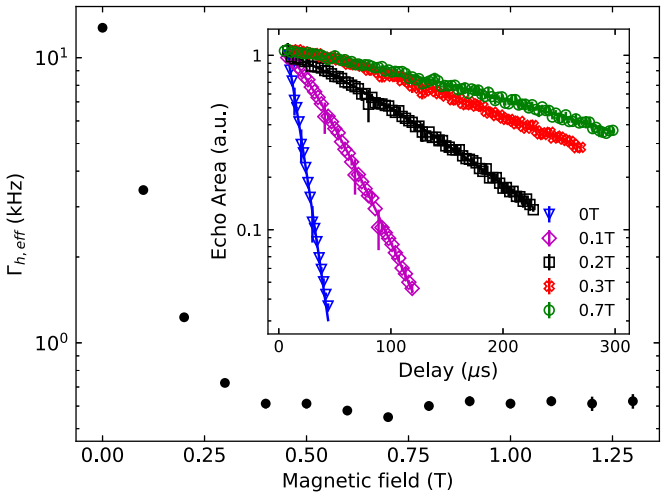

FIG. 2. Magnet field dependence of the effective homogeneous linewidth. We see the linewidth decrease from 12.5 kHz at 0 T down to 580 Hz at 0.7 T, where the linewidth saturates due to decoherence caused by TLS and superhyperfine interactions. Inset: Normalized echo decays at various fields.

includes contributions from hyperfine interactions between the $^{167}Er^{3+}$ (22.8% natural abundance) electron spin and its nuclear spin of 7/2. Additionally for ceramics, there may be magnetic impurities added during the manufacturing process that could increase $\Gamma_{\text{ion-spin}}$.

Γ_{TLS} is the dephasing that arises from fluctuations in the local environment (e.g., magnetic, electric fields) due to tunneling between two configurations with similar energy, known as tunneling two-level systems (TLS) [30,31]. For Er^{3+}-doped systems with TLS, two types of TLS have been observed [32]. One is the elastic TLS modes, which are independent of magnetic field. Another is the coupling between the large anisotropic magnetic moment of Er^{3+} and the elastic TLS modes, facilitated through elastic-dipole interactions [33], which we refer to as magnetic TLS. Magnetic TLS noise is expected to decrease with applied magnetic field, as opposed to elastic TLS which is field independent [32]. Γ_{TLS} is often the dominating contributor in amorphous solids [18,34,35], although to a lesser degree in ceramics as compared to glasses. Effects of TLS has been observed in other ceramics [23], and is likely contributing to this material as well. Γ_{phonon} includes spin relaxation caused by three primary phonon scattering processes: the direct one-phonon process, and the two-phonon Raman and Orbach processes [10,36].

In order to determine the contributions from these possible broadening mechanisms, the following sections investigate the various dependencies of the optical coherence.

C. Field dependence of Γ_h

Γ_h at increasing magnetic fields along the maximum absorption line are plotted in Fig. 2. We observed a decrease in linewidth from 12.5 kHz at zero field, to a minimum of 580 ± 20 Hz at 0.7 T. The uncertainty is extracted from the fit as one standard deviation. The linewidth does not change at higher fields. The reduction of Γ_h with field is indicative of decrease in both Er^{3+}-Er^{3+} flip-flops and magnetic TLS. The subsequent saturation of Γ_h is indicative of both the superhyperfine limit and elastic TLS. The measured homogeneous linewidth of 580 Hz is about an order of magnitude narrower than previously measured transparent ceramics [15,18], though it is still broader than the T_1-limited value of 22 Hz.

Between magnetic fields of 0.01 to 0.1 T, we observed periodic modulations in the echo amplitudes with τ, due to superhyperfine interactions between the electronic spin of Er^{3+} and nuclear spin of Y^{3+}. These oscillations decreased in amplitude and increased in frequency as the field was increased from 0.01 to 0.1 T. The modulation frequency was estimated to be about 100 kHz at 0.05 T. Two pulse echoes done on $Er^{3+}Y_2SiO_5$ show similar oscillations below 0.1 T [29]. These strong oscillations prevented accurate fitting and extraction of x parameter and T_M.

D. Temperature dependence of Γ_h

To further investigate the dephasing mechanisms, we measured the temperature dependence of homogeneous linewidth at 0.1 and 0.7 T, as shown in Figs. 3(a) and 3(b), respectively. At temperatures under 1 K, we see a linear increase of linewidth with temperature, characteristic of TLS being the dominating dephasing mechanism [30,31,37,38], without any increasing contributions from phonons. At higher temperatures (> 4 K), nonlinear behavior attributed to phonon scattering processes would be expected [15], but we did not measure in that temperature range due to limitations of our setup. Note that below 100 mK, we see a slight nonlinear plateau. This is likely due to the saturation of linewidth caused by coherently coupled TLS pairs [39], which dominate once the temperature falls under 100 mK where phonon scattering is very weak. It is also possible that the thermal conduction between the sample and the MXC is reduced at these temperatures, so the actual temperature of the sample deviated from the MXC temperature.

We perform a linear fit in Fig. 3 (excluding the points below 100 mK), according to

$$\Gamma_{\text{eff}} = \Gamma_0 + \alpha_{\text{TLS}} T, \tag{5}$$

where Γ_0 is the linewidth at 0 K. We obtain fit parameters of $\Gamma_0 = 4.8$ kHz and $\alpha_{\text{TLS}} = 7.8$ kHz/K at 0.1 T, and $\Gamma_0 =$ 320 Hz and $\alpha_{\text{TLS}} = 3.6$ kHz/K at 0.7 T. We first note that the TLS coupling α_{TLS} is halved at the higher field. The reduction in α_{TLS} is likely due to a reduction of magnetic TLS, which have been seen in similar systems [39,40]. Some TLS couples to the strong dipole moment of Er^{3+}, and the subsequent application of magnetic field decouples the two energy levels that constitute the TLS. This leads to lower tunneling rate, thus reducing the magnetic noise caused by TLS. We also note that $\Gamma_0 = 320$ Hz is the linewidth in the absence of TLS.

E. Spectral diffusion

To determine the temporal dependence of the linewidth, we investigate spectral diffusion using stimulated photon echoes (three pulse echoes). Three identical 300 ns pulses were sent, with a delay between the second and third pulse which we denote as the wait time T_w. The delay between the first and

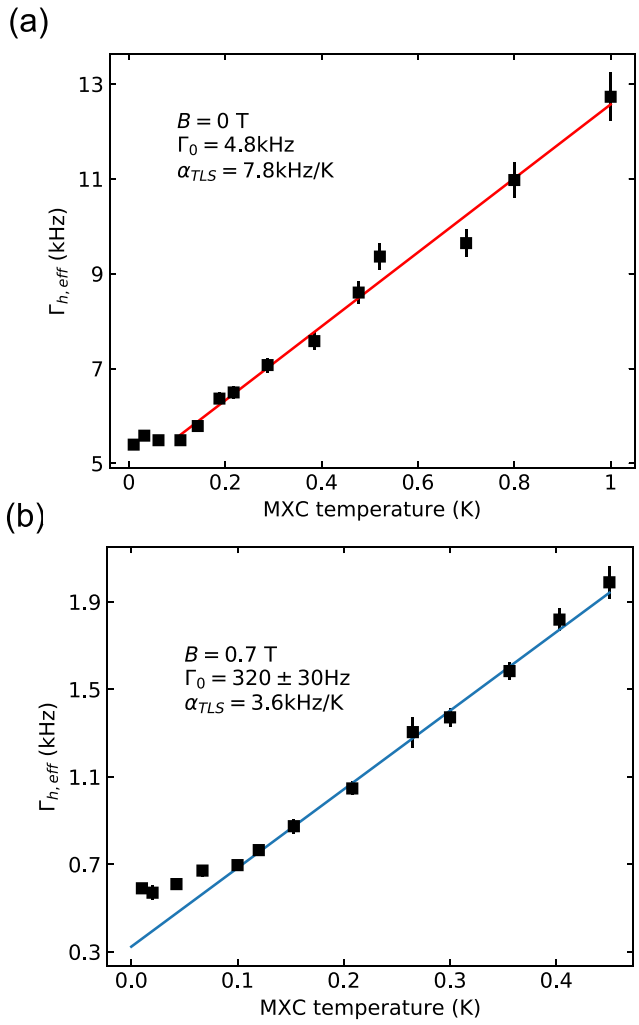

FIG. 3. (a) Temperature dependence of the homogeneous linewidth at 0.1 T. The linearity indicates decoherence dominated by TLS. The saturation at temperatures below 100 mK is also characteristic of coupled TLS pairs. (b) The same measurements at 0.7 T. We see decrease in both α_{TLS} and Γ_0.

second pulse τ was varied to extract the coherence time for a given T_w.

Spectral diffusion caused by spin flips and TLS is described by

$$\Gamma_h(T_w) = \gamma_0 + \frac{1}{2}\gamma_{SD}[1 - \exp(-RT_w)] + \gamma_{\mathrm{TLS}}\log\left(\frac{T_w}{t_0}\right), \tag{6}$$

where γ_0 is the homogeneous linewidth in the absence of spectral diffusion, γ_{SD} is the broadening due to magnetic spin flips, R is the perturbing spin flip rate, γ_{TLS} is the TLS coupling strength, and t_0 is the minimum measurement timescale, which is 10 μs. Here we take into account the contribution to spectral diffusion from the superhyperfine/hyperfine spin flips, indicated by the exponential term [10], and from TLS, given by the logarithmic term [34,35,41–43].

We use Eq. (6) to fit the three pulse echo decays, and the data and fit at $B = 0.5$ T is shown in the inset of Fig. 4. We obtain fit parameters of $\gamma_0 = 0.6$ kHz, $\gamma_{SD} = 1.8$ kHz,

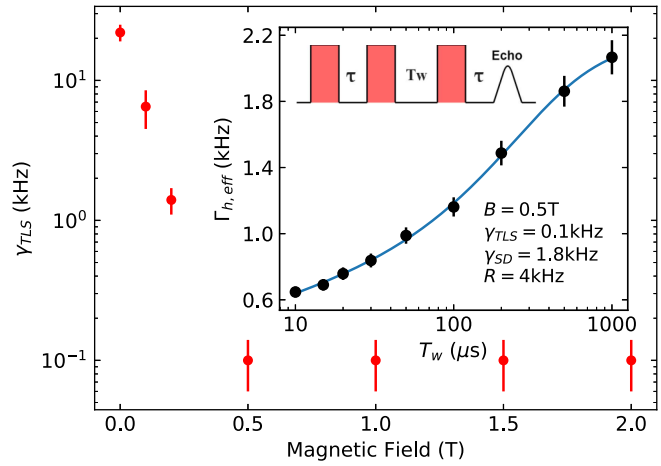

FIG. 4. Magnetic field dependence of the γ_{TLS}, measured with three pulse photon echoes. Inset: Spectral diffusion at 0.5 T, showing broadening from magnetic spin flips and TLS. The blue solid line is a fit to Eq. (6).

$R = 4$ kHz, and $\gamma_{\mathrm{TLS}} = 0.11$ kHz. At $B = 0$, the fit parameters were $\gamma_0 = 22$ kHz, $\gamma_{SD} = 2.0$ kHz, $R = 4$ kHz, $\gamma_{\mathrm{TLS}} = 20$ kHz. The reduction in γ_{TLS} is likely due to a reduction of magnetic TLS, as evident from the temperature dependence study. We saw no significant change in the diffusion rate with further increase in the field beyond 0.5 T. We also note that our value of γ_{TLS} at $B = 0.5$ T is about an order of magnitude smaller than those measured in Eu^{3+}:Y_2O_3 ceramics [18], mostly due to a significantly lower temperature in the current measurement.

Next, we consider the x parameter obtained from the Mims fit of the two pulse photon echo decays, which describes spectral diffusion. For all magnetic fields, x was approximately 1.2–1.3. Previous studies on Er^{3+}-doped glasses that have shown decoherence dominated by TLS reveal x parameters equal to or less than 1 [44,45]. Meanwhile, crystalline Er^{3+}:Y_2O_3 at the superhyperfine limit has shown $x = 1.4$ [1]. Therefore, it is probable that $x = 1.2$ arises from a combination of dephasing due to TLS and Er^{3+}-Y^{3+} superhyperfine interactions, and the linewidth beyond 0.7 T is limited by both mechanisms.

F. Summary of dephasing mechanisms

Here we provide a summary of the dephasing mechanisms uncovered by the various experiments. At low magnetic fields there is a combination of dephasing due to TLS, Er^{3+}-Er^{3+} interactions, and Er^{3+}-Y^{3+} interactions. The application of magnetic field above 0.7 T effectively suppressed the optical dephasing from Er^{3+}-Er^{3+} flip-flops and magnetic TLS.

For ceramics with such a narrow linewidth, it is plausible that charges on the boundaries between crystallite grains contributes some Stark broadening to the homogeneous linewidth. The Stark broadening was significant in Eu^{3+}:Y_2O_3 nanoparticles in [13], where they estimated a few kHz broadening from the Stark shift from charges on the surface of the nanoparticles. Following the same methods as [13] to calculate the possible contributions from charges on the grain

boundaries given submicron sized crystallites, we obtain tens of kHz of broadening. Because the expected broadening is much larger than our observed linewidth, we believe that there is no Stark broadening due to charges on crystalline boundaries. This is in line with the prediction in [13] for Eu^{3+}:Y_2O_3 nanoparticles, where the charge fluctuations are thought to be from the surface of the nanoparticles, rather than interfaces between the crystallites.

For the remaining linewidth of about 560 Hz above 0.7 T (after subtraction of the T_1 contribution), from the results of Fig. 3(b), we attribute approximately 300 Hz for Er^{3+}-Y^{3+} superhyperfine interactions and possible $^{167}Er^{3+}$ hyperfine interactions. We are left with 260 Hz due to elastic TLS. Part of the superhyperfine interactions could come from the frozen core, where the large magnetic moment of Er^{3+} slows the flipping of nearby yttrium nuclear spins.

IV. CONCLUSION

In this work we characterized spectroscopic properties of polycrystalline Er^{3+}:Y_2O_3 ceramics at dilution temperatures. We achieved the narrowest optical homogeneous linewidth of 580 Hz of rare-earth doped ceramics, and measured a low spectral diffusion of ∼2 kHz over 1 ms. Through systematic investigation of Γ_h, we conclude that the limiting decoherence mechanisms are roughly equal parts elastic TLS and superhyperfine interactions between Er^{3+} and Y^{3+} nuclear spins. This suggests that the ceramic exhibits properties of a combination of amorphous solids, in which decoherence is limited by TLS [44], and single crystals [10] where decoherence is limited by superhyperfine interactions with the host. The understanding of relevant dephasing mechanisms informs further works to extend the Er^{3+} coherence lifetimes. With refined synthesis processes, Er^{3+}:Y_2O_3 ceramics with larger grain sizes (e.g., on the order of a few microns) could yield narrower linewidths as dephasing experienced by ions far from TLSs on the grain boundaries is reduced. On the other hand, enhanced coupling to long-lived TLS in smaller ceramic grains can be exploited to realize new hybrid systems. An isotopically purified version of this sample with $^{167}Er^{3+}$ would allow us to potentially attain long spin coherence lifetimes by performing spin initialization into a non-Boltzmann hyperfine state and suppressing noise due to nuclear spin cross relaxations [5]. Our study indicates that transparent Er^{3+}:Y_2O_3 ceramics is a versatile and promising material for developing long-coherence quantum systems in the technologically relevant telecom band.

ACKNOWLEDGMENTS

We are grateful to C. W. Thiel and J. G. Bartholomew for valuable discussions. We acknowledge equipment support from the National Science Foundation Grant No. ECCS-1843044. Y.H. acknowledges the support from the Argonne National Laboratorys Laboratory Directed Research and Development (LDRD) program.

R.F. and Y.H. contributed equally to the experiments.

[1] C. Thiel, T. Böttger, and R. L. Cone, J. Lumin. **131**, 353 (2011).
[2] R. W. Equall, Y. Sun, R. L. Cone, and R. M. Macfarlane, Phys. Rev. Lett. **72**, 2179 (1994).
[3] M. Zhong, M. P. Hedges, R. L. Ahlefeldt, J. G. Bartholomew, S. E. Beavan, S. M. Wittig, J. J. Longdell, and M. J. Sellars, Nature (London) **517**, 177 (2015).
[4] T. Böttger, C. W. Thiel, R. L. Cone, and Y. Sun, Phys. Rev. B **79**, 115104 (2009).
[5] M. Rančić, M. P. Hedges, R. L. Ahlefeldt, and M. J. Sellars, Nat. Phys. **14**, 50 (2018).
[6] B. Lauritzen, J. Minář, H. de Riedmatten, M. Afzelius, and N. Gisin, Phys. Rev. A **83**, 012318 (2011).
[7] H. J. Kimble, Nature (London) **453**, 1023 (2008).
[8] G. Kurizki, P. Bertet, Y. Kubo, K. Mølmer, D. Petrosyan, P. Rabl, and J. Schmiedmayer, Proc. Natl. Acad. Sci. **112**, 3866 (2015).
[9] C. L. Degen, F. Reinhard, and P. Cappellaro, Rev. Mod. Phys. **89**, 035002 (2017).
[10] T. Böttger, C. W. Thiel, Y. Sun, and R. L. Cone, Phys. Rev. B **73**, 075101 (2006).
[11] T. Zhong and P. Goldner, Nanophotonics **8**, 2003 (2019).
[12] M. Scarafagio, A. Tallaire, K.-J. Tielrooij, D. Cano, A. Grishin, M. H. Chavanne, F. H. Koppens, A. Ringuedé, M. Cassir, D. Serrano, P. Goldner, and A. Ferrier, J. Phys. Chem. C **123**, 13354 (2019).
[13] J. G. Bartholomew, K. de Oliveira Lima, A. Ferrier, and P. Goldner, Nano Lett. **17**, 778 (2017).
[14] D. Serrano, C. Deshmukh, S. Liu, A. Tallaire, A. Ferrier, H. de Riedmatten, and P. Goldner, Phys. Rev. B **100**, 144304 (2019).
[15] H. Zhang, J. Yang, S. Gray, J. A. Brown, T. D. Ketcham, D. E. Baker, A. Carapella, R. W. Davis, J. G. Arroyo, and D. A. Nolan, ACS Omega **2**, 3739 (2017).
[16] R. Macfarlane and R. Shelby, Opt. Commun. **39**, 169 (1981).
[17] A. Perrot, P. Goldner, D. Giaume, M. Lovrić, C. Andriamiadamanana, R. R. Gonçalves, and A. Ferrier, Phys. Rev. Lett. **111**, 203601 (2013).
[18] N. Kunkel, J. Bartholomew, S. Welinski, A. Ferrier, A. Ikesue, and P. Goldner, Phys. Rev. B **94**, 184301 (2016).
[19] Y. Sun, T. Böttger, C. W. Thiel, and R. L. Cone, Phys. Rev. B **77**, 085124 (2008).
[20] T. L. Harris, Ph.D. thesis, Montana State University, Bozeman, Montana, 2001.
[21] N. Kukharchyk, D. Sholokhov, O. Morozov, S. Korableva, A. Kalachev, and P. Bushev, New J. Phys. **20**, 023044 (2018).
[22] I. Craiciu, M. Lei, J. Rochman, J. M. Kindem, J. G. Bartholomew, E. Miyazono, T. Zhong, N. Sinclair, and A. Faraon, Phys. Rev. Appl. **12**, 024062 (2019).
[23] A. Ferrier, C. W. Thiel, B. Tumino, M. O. Ramirez, L. E. Bausá, R. L. Cone, A. Ikesue, and P. Goldner, Phys. Rev. B **87**, 041102(R) (2013).
[24] B. D. Bartolo, *Optical Interactions in Solids* (Wiley, New York, 1968).
[25] B. Henderson and G. F. Imbusch, *Optical Spectroscopy of Inorganic Solids* (Oxford University Press, Oxford, 2006).

[26] G. Liu and B. Jacquier, Eds., *Spectroscopic Properties of Rare Earths in Optical Materials* (Tsinghua University Press, Beijing, 2010).
[27] W. B. Mims, Phys. Rev. **168**, 370 (1968).
[28] G. K. Liu and R. L. Cone, Phys. Rev. B **41**, 6193 (1990).
[29] B. Car, L. Veissier, A. Louchet-Chauvet, J.-L. Le Gouët, and T. Chanelière, Phys. Rev. Lett. **120**, 197401 (2018).
[30] P. W. Anderson, B. I. Halperin, and C. M. Varma, Philos. Mag. **25**, 1 (1972).
[31] W. A. Phillips, J. Low Temp. Phys. **7**, 351 (1972).
[32] R. Macfarlane, Y. Sun, P. Sellin, and R. Cone, J. Lumin. **127**, 61 (2007).
[33] D. L. Huber, M. M. Broer, and B. Golding, Phys. Rev. Lett. **52**, 2281 (1984).
[34] J. L. Black and B. I. Halperin, Phys. Rev. B **16**, 2879 (1977).
[35] W. Breinl, J. Friedrich, and D. Haarer, J. Chem. Phys. **81**, 3915 (1984).
[36] Y. Sun, C. W. Thiel, and R. L. Cone, Phys. Rev. B **85**, 165106 (2012).
[37] G. P. Flinn, K. W. Jang, J. Ganem, M. L. Jones, R. S. Meltzer, and R. M. Macfarlane, Phys. Rev. B **49**, 5821 (1994).
[38] R. Macfarlane, Y. Sun, R. Cone, C. Thiel, and R. Equall, J. Lumin. **107**, 310 (2004), Proceedings of the 8th International Meeting on Hole Burning, Single Molecule, and Related Spectroscopies: Science and Applications.
[39] D. Ding, D. van Driel, L. M. C. Pereira, J. F. Bauters, M. J. R. Heck, G. Welker, M. J. A. de Dood, A. Vantomme, J. E. Bowers, W. Löffler, and D. Bouwmeester, Phys. Rev. B **101**, 014209 (2020).
[40] M. U. Staudt, S. R. Hastings-Simon, M. Afzelius, D. Jaccard, W. Tittel, and N. Gisin, Opt. Commun. **266**, 720 (2006).
[41] K. A. Littau, M. A. Dugan, S. Chen, and M. D. Fayer, J. Chem. Phys. **96**, 3484 (1992).
[42] R. Silbey, J. Koedijk, and S. Völker, J. Chem. Phys. **105**, 901 (1996).
[43] J. Koedijk, R. Wannemacher, R. Silbey, and S. Völker, J. Phys. Chem. **100**, 19945 (1996).
[44] L. Veissier, M. Falamarzi, T. Lutz, E. Saglamyurek, C. W. Thiel, R. L. Cone, and W. Tittel, Phys. Rev. B **94**, 195138 (2016).
[45] T. Lutz, L. Veissier, C. W. Thiel, P. J. Woodburn, R. L. Cone, P. E. Barclay, and W. Tittel, J. Lumin. **191**, 2 (2017).